IL NUOVO CIMENTO Vol. 31 C, N. 5-6 Settembre-Dicembre 2008
DOI 10.1393/ncc/i2009-10331-x

Comparison of structure function and detrended fluctuation analysis of wind time series

A. M. Tarquis(1)(2)(*), M. C. Morató(2), M. T. Castellanos(2) and Alicia Perdigones(3)

(1) *CEIGRAM, Universidad Politécnica de Madrid (UPM) - Madrid, Spain*
(2) *Departamento de Matemática Aplicada en Ingeniería Agronómica, ETSI Agrónomos UPM - Madrid, Spain*
(3) *Departamento de Ingeniería Rural, ETSI Agrónomos, UPM - Madrid, Spain*

(ricevuto il 28 Settembre 2008; approvato il 23 Dicembre 2008; pubblicato online il 6 Maggio 2009)

Summary. — A multifractal (MF) analysis in time scale has been applied to three wind speed series presenting a different pattern. The temporal scaling properties of the records, registered each 10 minutes, were studied using two different methods, structure function (SF) and detrended fluctuation analysis (DFA), to establish a comparison of the results and their interpretation in the geostrophic turbulence context. A systematic analysis of the exponent of the structure function ($\zeta(q)$) and the generalized Hurst exponents ($H(q)$) gave, in general terms, equivalent results when a comparison is applied among the three months. However MF DFA presented statistically more robust results. This allowed us to see a clear difference between the parameters studied for each month: linear component of $\zeta(q)$ ($\zeta(q=1)=H$), intermittency of the wind series (μ), deviation from linear structure function (λ), Hurst exponent ($H(q=2)$) and $H(q)$ dependence on q (ΔH).

PACS 89.60.-k – Environmental studies.
PACS 87.10.Mn – Stochastic modeling.

1. – Introduction

Many time series show pronounced cyclic trends. For example, daily temperature data follow an annual cycle whose magnitude overwhelms other fluctuations; rainfall data in many areas undergoes a similar annual cycle of similar magnitude as well as wind velocity data (v) [1]. For most practical applications, such as engineering and meteorology, one mainly distinguishes between large-scale variations such as diurnal, weekly and seasonal changes and variations on small scales often referred to as atmospheric turbulence or

(*) E-mail: anamaria.tarquis@upm.es

gustiness [2]. The existence of a mesoscale gap as proposed by Van der Hoven [3], which divides micro, and macro scales in a more rigorous way has strongly been debated in recent years [4-6].

With a wind time series recorded each 10 minutes, at 1.5 m from the surface, we are studying mainly diurnal variations. In both tropical and temperate latitude, large wind variations can occur on a diurnal or daily time scale. This differential heating of the Earth's surface during the variation is an increase in wind speed during the day, with wind speeds lowest during the hours from midnight to sunrise. Daily variations in solar radiation are responsible for diurnal wind variations in temperate latitudes over relatively flat land areas. The largest diurnal changes generally occur in spring and summer, and the smallest in the winter. This case study is in a quite different scenario from the ones showed by Yagüe *et al.* [6] and Vindel *et al.* [7].

In the last few decades there has been an increasing recognition that multiplicative cascades combined with multiscaling analysis represent extremely useful tools for characterizing a variety of geophysical signals [8-11] and hourly wind speed [12]. Cascade model generates signals by dividing an interval assigned a single value into an integer number of parts, and assigning each new interval a new value, usually some random ratio of the initial value. This process is then iterated on each new interval, and so on. The resulting data can be described by the multifractal formalism [13, 14] and can be characterized with the use of multiscaling analysis, which determines the dependence of the statistical moments on the resolution with which the data are examined [15]. In some way, Frisch and Parisi [13] introduced the idea to understand many geophysical time series data as a chaotic process.

A stochastic fractal representation of wind speed was introduced by Schmitt *et al.* [16] via the notion of universal multifractals [17, 18]. Their idea is to represent time series as a realization of a Levy process and parameterize it via its codimension function. Even though reasonable looking simulations having intermittency, as found in wind speed and rainfall, may be obtained a demand for reliable predictions has been growing lately [19]. This type of analysis has important implications on the understanding of wind speed patterns and shows this variable to be more heterogeneous than is usually modelled.

The study of v is aimed for several agronomic applications. For example, at greenhouse control (heating and ventilation), since wind velocity influences both types of control. Wind increases heat losses in winter nights, so it is of interest to regulate the heating as a function of wind-speed (v). With respect to ventilation, the opening of the windows must be reduced with high values of wind velocity [20]. There are several automatisms and algorithms regulating all these processes and to simulate different scenarios to test them is one of the essential steps in the optimization process. These models and relationships make the identification of patterns in the wind's behaviour very interesting. It is therefore desirable to compare the wind speed on a given date to the average of the wind speed on that date [11, 21, 22].

The aim of this work is to study wind speed time series data using two powerful techniques called Structure Function (SF) [16, 23] and Multifractal Detrended Fluctuation Analysis (DFA) [12, 24]. The methods provide a systematic means to identify and more importantly quantify the multiple scaling exponents in the data [24]. The scaling exponents of the data are estimated under the assumption of a binomial multiplicative cascade model. This is carried out on the wind speed data acquired from three different months at a monitoring location in Madrid, Spain. In this way, it is possible to fully characterize the dynamical system and to simulate at high resolution (interval of 10 minutes) monthly wind speed fluctuations series at a geostrophical scale.

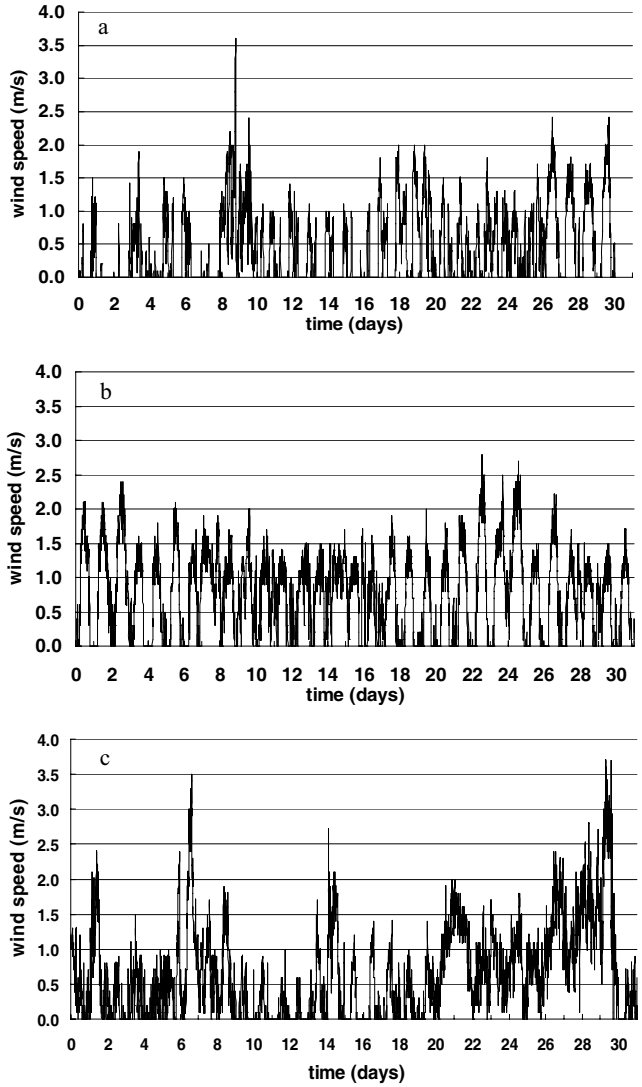

Fig. 1. – Original data of wind speed during (a) June, (b) July and (c) December 2004 recorded each 10 minutes.

2. – Data

Wind speeds are registered through a climatic station of *Dpto. de Producción Vegetal: Botánica y Protección de Cultivos*, placed in the experimental fields of the Agricultural School of Madrid. This station is based on a METEODATA-256 unit of *Geónica, S.A.* placed exactly at 40° 26′ 36″ N; 3° 44′ 18″ W and 595 m of altitude.

The central unit of Meteodata-256 stores the instant values coming from the sensors, located 1 m over the land surface, each 10 seconds in a volatile memory and each 10 minutes made an average and transfer the results to a data base through a RS232-C line [25].

We used times series data from 2004 (see fig. 1). Thus we handle in each monthly analysis a minimum of 4160 values and a maximum of 4464.

3. – Multifractal analysis

Conventionally, the statistical modelling of wind speed data has been done by using Weibull and Rayleigh probability distribution functions [26]. While these methods are useful in providing estimates of wind generated energy yield, they do not explicitly bring out the nature of the temporal variations in wind speed [12]. Complex motions in the atmosphere tend to render the wind speed distinctly non-stationary and intermittent. Power spectral techniques have been used successfully to detect possible long-range correlations of the form $S(f) \sim 1/f^{\beta}$ [27]. Long-range correlations generally indicate that temporally well-separated samples of the time series are correlated with each other and indicative of self-similar behaviour. Self-similar time series can be characterized by

$$y(t) \equiv a^{H(2)} y(t/H(2)), \tag{1}$$

where the $\equiv$ in eq. (1) denotes that both sides of the equation have identical statistical properties. The exponent $H(2)$ in eq. (1) is called the self-similarity parameter, or the Hurst exponent. The exponent (β) estimated from the power spectrum ($S(f) \sim 1/f^{\beta}$) is related to $H(2)$ as $\beta = 2H(2) + 1$. The temporal trace and corresponding power spectrum of each of the studied month are shown in fig. 2. Estimating the Hurst exponent ($H(2)$) from the given data is an alternate effective way to determine the nature of the correlations in it [28]. Hurst exponents have been successfully used to quantify long-range correlations in plasma turbulence [29,30], finance [31,32], network traffic [33], and physiology [34]. Long-range correlations or persistence are said to exist if $0.5 < H(2) < 1$, see Beran [35] and Bassingthwaighte [36] for details. Values of $H(2)$ in the range of $0 < H(2) < 0.5$ characterize anti-persistence, whereas those with $H(2) = 0.5$ represent uncorrelated noise.

Hurst estimators are susceptible to such artifacts such as polynomial trends which cannot be ruled out in experimental data and therefore, they may give spurious results. It should be noted that the techniques listed above can only extract a single scaling exponent from a time series. However, it is possible that the given process may be governed by more than one scaling exponent, in which case a single scaling exponent would be unable to capture the complex dynamics inherent in the data. Therefore, these methods are appropriate only for the analysis of monofractal signals which have uniform scaling properties throughout the signal which can be characterized by a single exponent. On the other hand, multifractal signals are far more complex than monofractal signals and require more than one (theoretically infinite) exponent to characterize their scaling properties [34].

3˙1. *Structure function.* – For nonstationary processes, $v(t)$, with stationary increments, the Structure Function (SF) of order q is defined as the q-th moment of the increments of $v(t)$ by the following equation:

$$M_q(\tau) \equiv \left\langle \left| v(t_{i+\tau}) - v(t_i) \right|^q \right\rangle, \tag{2}$$

where i denotes the i-th data point, and $\langle\ \rangle$ denotes the ensemble average. Structure functions are generalized correlation functions, which is particularly evident from eq. (2) for the case of $q = 2$. In general, q may be any real number not just integers, and can even be negative. However, there are divergence problems inherent to the negative-order exponent so that computations are best restricted to positive real number [9]. If the

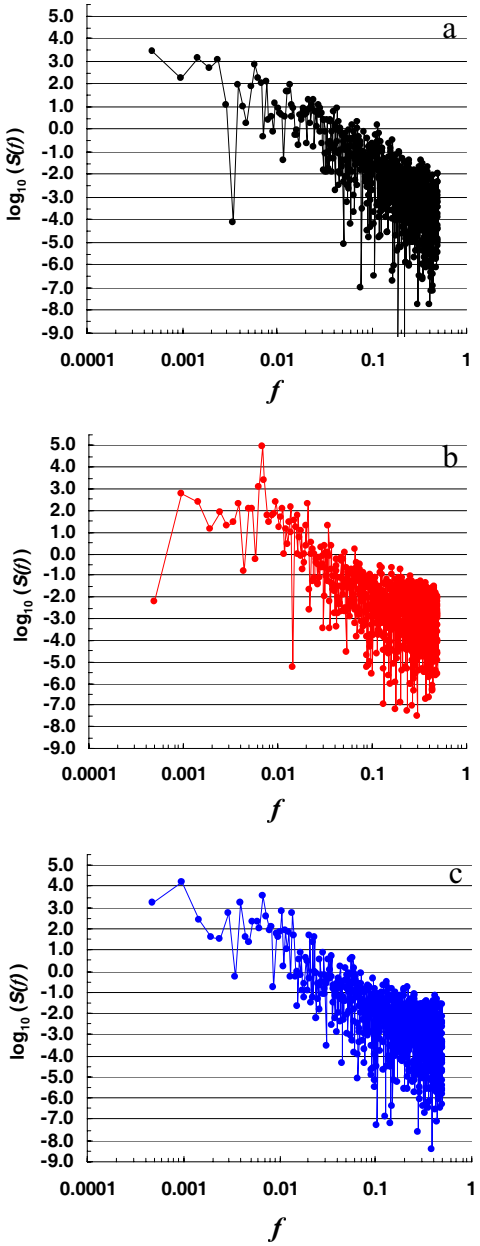

Fig. 2. – Spectral analysis for each month using the first 2046 data points: a) June, b) July and c) December 2004.

process $v(t)$ is scale-invariant and self-similar or self-affine over some range of time lags $\tau_{\min} \leq \tau \leq \tau_{\max}$, then the q-th-order structure function is expected to scale as

$$M_q(\tau) = C_q \tau^{\zeta(q)}, \tag{3}$$

where C_q can be a function of τ which varies more slowly than any power of τ, and $\zeta(q)$ is the exponent of the structure function. $\zeta(q)$ is a monotonically non-decreasing function of q if $v(t)$ has absolute bounds [14, 18]. From eq. (3) we can see that the statistics of the fluctuations over time lags τ has two components; the first because it depends on the fluctuations at low τ values, the second because of the scaling relation between the fluctuations and τ.

The behaviour described by eq. (2) and eq. (3) is called "multiscaling" because each statistical moment is scaling but with a different exponent. Therefore, a hierarchy of exponents can be defined using $\zeta(q)$:

$$H(q) = \frac{\zeta(q)}{q}\,, \tag{4}$$

where $H(q)$ is the generalized Hurst exponent (or self-similarity scaling exponent) [9]. Calculation of $H(q)$ allows the straightforward identification of persistence, or long-time correlation, as well as the stationary/nonstationary and monofractal/multifractal nature of the data [5]. Stationary processes have scale-independent increments and $\zeta(q) = H(q) \equiv 0$, due to the invariance under translation. Processes with a linear $\zeta(q)$ (or a constant $H(q)$) are monofractal, otherwise they are non-stationary and multifractal.

Taking the famous Kolmogorov [37] law for homogeneous and isotropic turbulence in local equilibrium (named K41 theory), established the following relation between the spatial structure functions S_q and spatial scales (l):

$$M_q(l) \propto \langle\varepsilon\rangle^{q/3} l^{q/3}, \tag{5}$$

where $\langle\varepsilon\rangle$ is the mean energy dissipation rate assuming that it does not vary in space nor time. Nonlinearity with a scaling exponent of the order q of the statistical moment has been observed in many theoretical, experimental and numerical investigations ([38]; [6] and references therein). In fact, Frisch [13] indicated that the average value of the energy dissipation will be different at different points in space correcting K41 theory and this correction is referred to as intermittency.

The spatial and temporal descriptions of the cascade may be exchanged assuming Taylor's "frozen eddy" hypothesis, then we can formulate a relation between energy flux (ε) to velocity fluctuations (Δv) over a time Δt as follows:

$$\Delta v_\tau(\Delta t) = \varepsilon_\tau^a \Delta t^H; \qquad \Delta t = \tau_{\max}/\tau. \tag{6}$$

The usual interpretation of this equation is that the equality is in the sense of scaling laws so that, taking the q-th powers of both sides and ensemble averaging, we obtain [39]

$$\langle \Delta v_\tau^q \rangle \propto \langle \varepsilon_\tau^{aq} \rangle \tau^{qH} \propto \tau^{\zeta(q)}. \tag{7}$$

In this expression we do not force H to be equal to 1/3. We can see that the fluctuations of typical observables have a linear (qH) and nonlinear scaling term. The generalized structure function exponent $\zeta(q)$ is achieved in a similar way to eq. (3) coming from a turbulence background (the usual structure function for $q = 2$, is called a "variogram"). From eq. (6) we can see that the statistics of the fluctuations over times Δt has two components; the first because it depends of the flux ε at low lag times $\tau = \tau_{\max}/\Delta t$, the second because of the scaling relation between the fluctuations and the flux (Δt^H).

From turbulence point of view, H characterizes the difference from the (conserved) pure multiplicative process ε; it is the degree of non (scale by scale) conservation of the process.

The standard definition of intermittency (μ) uses the sixth-order structure function or $\zeta(q = 6)$ when the scaling is in space [39-41] but we have to adapt it in time scaling so the units correspond for both parts of the relation. Following Mahrt [40] work the dissipation correlation function could be expressed as

$$\langle \varepsilon(t_{i+\tau})\varepsilon(t_i)\rangle \propto \left(\frac{\tau_{\max}}{\tau}\right)^{\mu} \tag{8}$$

and it is related to the structure function based on time scaling as

$$\langle \varepsilon(t_{i+\tau})\varepsilon(t_i)\rangle \propto \frac{\langle(\Delta v)^4\rangle}{\tau^2}\,. \tag{9}$$

From eqs. (8) and (9), we see that the 4th-order structure function is related to μ by

$$\left\langle(\Delta v)^4\right\rangle \propto \tau^{2-\mu} \qquad \text{or} \qquad \mu = 2 - \zeta(q = 4). \tag{10}$$

We have defined another parameter to reflect the deviation from a linear structure function (λ) as

$$\lambda = 4H - \zeta(q = 4) = 4\zeta(q = 1) - \zeta(q = 4). \tag{11}$$

In other words, the difference between a linear structure function qH, based on $\zeta(q = 1)$ value, and the one obtained for $q = 4$.

3˙2. *Multifractal DFA.* – It is worth noting that the fluctuation Δv_τ is sometimes called the "poor man's wavelet"; other choices of definition are possible; wavelets provide a systematic framework for this (see, *e.g.*, [42]). However, in practice, definition (2) is usually adequate, the main restriction being that it is only appropriate when $0 \leq H(2) \leq 1$, a condition which is usually (although not always) satisfied in geophysical applications. For example, when $H(2) > 1$, one must measure fluctuations with respect to a local linear trend; this can be done either by fractionally differentiating the process power law filtering, [23], using appropriate wavelets [43] or using the "Multifractal Detrended Fluctuation Analysis" technique [24]. We will apply the latest method.

The main feature of multifractals is that they are characterized by high variability on a wide range of temporal or spatial scales, associated to intermittent fluctuations and long-range power law correlations. To perform a multifractal analysis for all values of q, Kantelhardt *et al.* [24] have developed the DFA. A brief description of the algorithm is provided in this section.

The DFA operates on the time series $v(i)$, where $i = 1, 2, \ldots, N$ and N is the length of the series, with $\bar{v}$ we indicate the mean value

$$\bar{v} = \frac{1}{N}\sum_{k=1}^{N} v(k). \tag{12}$$

We assume that $v(i)$ are increments of a random walk process around the average $\bar{v}$, thus the "trajectory" or "profile" is given by the integration of the signal

$$y(i) = \sum_{k=1}^{i} \big[v(k) - \bar{v}\big]. \tag{13}$$

Furthermore, the integration will reduce the level of measurement noise present in observational and finite records. Next, the integrated time series is divided into $N_S = \mathrm{int}(N/s)$ non-overlapping segments of equal length s. Since the length N of the series is often not a multiple of the considered timescale s, a short part at the end of the profile $y(i)$ may remain. In order not to disregard this part of the series, the same procedure is repeated starting from the opposite end. Thereby, $2N_S$ segments are obtained altogether. Then we calculate the local trend for each of the $2N_S$ segments by a least-squares fit of the series. Then we determine the variance

$$F^2(s,n) = \frac{1}{s}\sum_{i=1}^{s}\Big\{y_{[(n-1)s+i]} - y_v(i)\Big\}^2 \tag{14}$$

for each segment n, being $n = 1, \ldots, N_S$ and

$$F^2(s,n) = \frac{1}{s}\sum_{i=1}^{s}\Big\{y_{[N-(n-N_s)s+i]} - y_v(i)\Big\}^2 \tag{15}$$

for $n = N_s + 1, \ldots, 2N_s$. Here, $y_v(i)$ is the fitting line in n segments. Then, after detrending the series, we average over all segments to obtain the q-th-order fluctuation function

$$F_q(s) = \left\{\frac{1}{2N_s}\sum \big[F^2(s,n)\big]^{q/2}\right\}^{1/q}, \tag{16}$$

where, in general, the index variable q can take any real value except zero. In our case, time series lengths were multiple of s and eq. (8) was not applied.

Repeating the procedure described above, for several timescales s, $F_q(s)$ will increase with increasing s. Then analysing log-log plots of $F_q(s)$ *vs.* s for each value of q, we determine the scaling behaviour of the fluctuation functions. If the series x_i is a long-range power law correlated, $F_q(s)$ increases for large values of s as a power law

$$F_q(s) \propto s^{H(q)}. \tag{17}$$

As mentioned above in last section, monofractal time series with compact support are characterized by $H(q)$ independent of q. The different scaling of small and large fluctuations will yield a significant dependence of $H(q)$ on q. The higher is this dependence the higher is the difference in scaling that we could quantify through ΔH, defined as

$$\Delta H = H(q = 0.5) - H(q = 6). \tag{18}$$

In this case, to obtain $\zeta(q)$ from the $H(q)$ obtained with DFA we applied eq. (4).

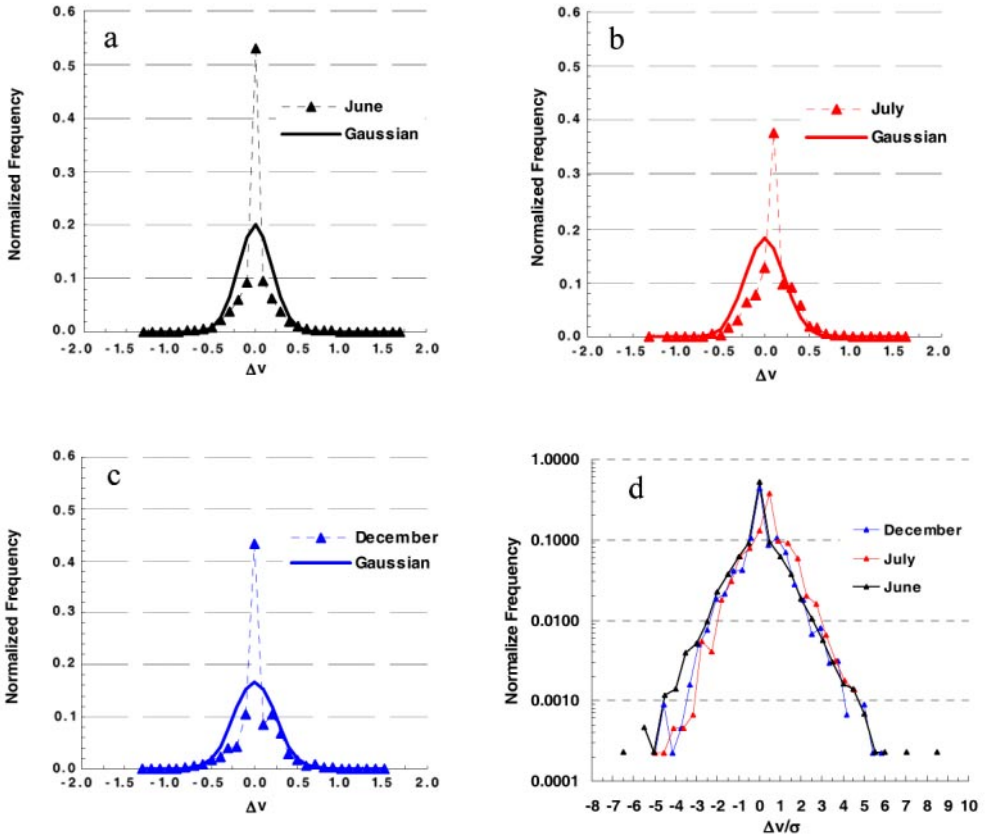

Fig. 3. – Normalized frequency of wind fluctuations for June, July and December 2004. Continuous line represents the Gaussian distribution using the average and standard deviation of the same wind fluctuation data.

4. – Results

4˙1. *Power spectrum and wind fluctuation.* – Looking at time series for each month there are some relevant features. July wind speed (fig. 1a) has a clear pattern close to 24 hours cycle pointing out the major effect of soil and diurnal temperatures. The graphic showing June time series (fig. 1a) at the beginning (from 0 to 400 hours) reveals a high heterogeneity and then shows the same behaviour as July. December time series shows a mix of scenarios with high intermittency and not a periodic pattern as July.

Spectral analysis or power spectrum for each month (fig. 2) points out the different highest point in the ordinates. It can be observed that frequencies around 24 hours are very important in the three months, however June shows another local maximum for each 3 days and December for each 2 days.

Wind fluctuation statistics are shown in fig. 3. For each month the difference between the data and a Gaussian distribution is clear (fig. 3a,b,c) mainly at null wind fluctuation that gives the highest frequency and the biggest difference from Gaussian distributions.

4˙2. *Multifractal SF.* – In this case we have used q values varying from 0.5 to +6 with an increment of 0.5. The numbers of points used in each regression line, obtained from

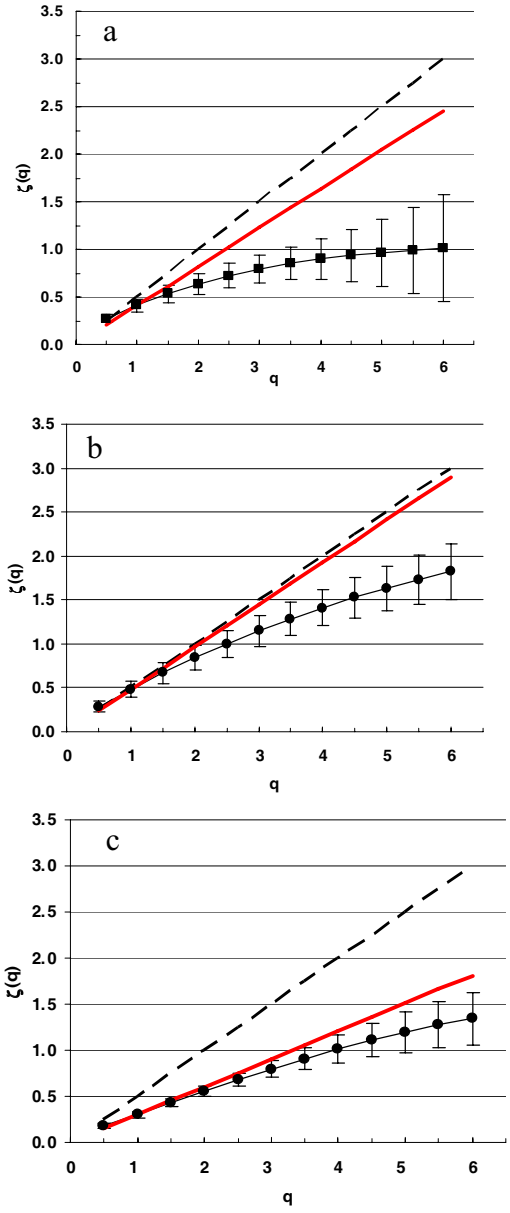

Fig. 4. – $\zeta(q)$ curves obtained by SF for a) June, b) July, c) December. Dashed line represents time series with uncorrelated noise (slope value of 0.5); grey line represents the linear part of $\zeta(q)$ having a constant slope with value $\zeta(q = 1)$.

eq. (3) taking natural logarithms, for a fixed q to estimate $\zeta(q)$ was always 6 points, corresponding to a lag time of 20 till 64 minutes (approximately one hour), that gave the best linear fit.

Using eq. (2) we obtain the generalized structure functions shown in fig. 4. We can see that except for the highest values of q, in which the errors are higher, the scaling

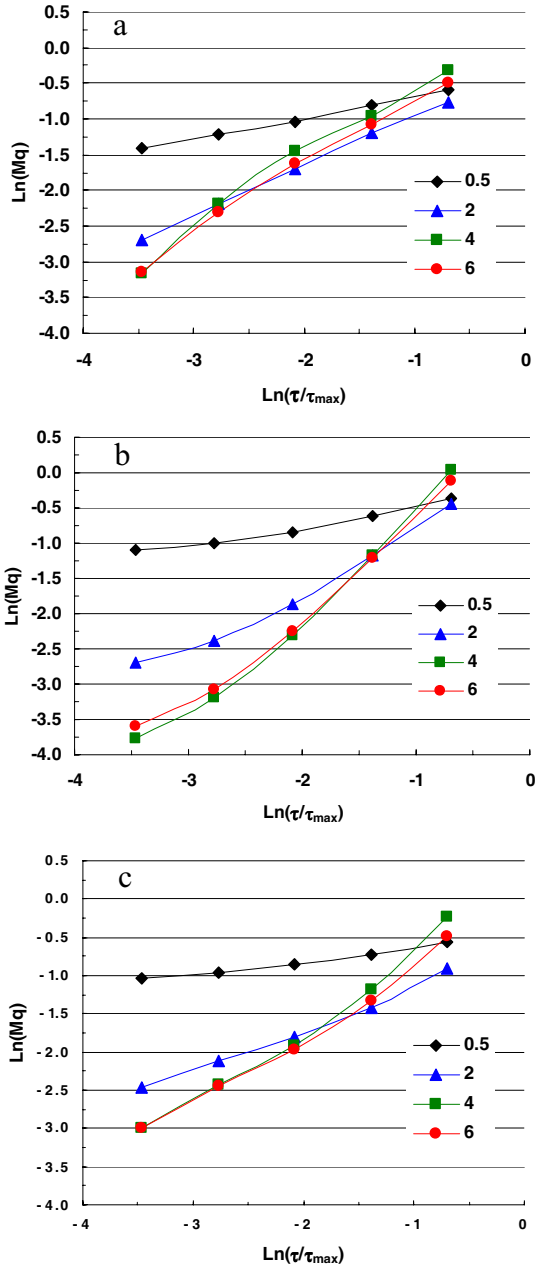

Fig. 5. – Structure functions (Mq) for $q = 0.5$, 2, 4 and 6 for (a) June, (b) July and (c) December 2004.

is excellent. In order to quantify the differences in the scaling, in fig. 5 we show the slopes which are our estimates of $\zeta(q)$. We can see that (as expected) $\zeta(q)$ is concave downwards. It is interesting to note that while June and July have a clear non-linear $\zeta(q)$, December presents a non-clear multifractality in $\zeta(q)$.

TABLE I. – $\zeta(q)$ *values from* $q = 1$ *(*H*),* $q = 4$ *and* $q = 6$*. Estimations have been made through the structure function (SF). Parameters estimated for intermittency* (μ) *and deviation from linear structure function* (λ)*.*

	$\zeta(q=1)$	$\zeta(q=4)$	$\zeta(q=6)$	μ	λ
June	0.41 ± 0.07	0.90 ± 0.21	1.01 ± 0.56	1.10 ± 0.21	0.74 ± 0.48
July	0.48 ± 0.09	1.41 ± 0.21	1.82 ± 0.31	0.59 ± 0.21	0.52 ± 0.50
December	0.30 ± 0.04	1.01 ± 0.15	1.35 ± 0.28	0.99 ± 0.15	0.20 ± 0.19

Table I shows the most important parameters we can extract to compare the three months, and reduce the problem to a finite number of manageable parameters. It is helpful to compare these H values with those of other geophysical fields. We can mention the classical Kolmogorov turbulent result and the clasical parameter for passive scalars in turbulence and the Corrsin-Obhukhov law, all of them with a value of 1/3. June and July are higher than this value meanwhile December is closer to it.

Respect to the deviation from linear structure function (λ) is gradually reduced from June to December (see table I), however due to $\zeta(q = 4)$ and $\zeta(q = 1)$ errors the differences are not clear. The intermittency parameter (μ) shows June and December with high values, even higher than the ones reported by previous works in the space scales [40, 41, 44] which showed values ranging from 0.15 till 0.50.

Another way to compare these three different scenarios is using $H(q)$ making a first quantification estimating the range of variation of $H(q)$ and given the Hurst exponent ($H(2)$). In table II we compare these estimates finding that over all 3 months Hurst exponent presents a clear anti-persistent character December being the lowest value and highlighting July as closer to an uncorrelated noise behaviour than June and December. To have a better idea on the variation of $H(q)$ values, these have been plotted using eq. (4) (fig. 6).

4˙3. *Multifractal DFA.* – In this method we have used the same range of q and τ values as in the previous method (SF) to establish a more clear comparison. Using eq. (16) to estimate the fluctuation of wind speed around a linear trend, we obtain the generalized Hurst exponent ($H(q)$) function shown in figs. 7a, 7b and 7c for June, July and December, respectively. We can see that comparing this set of graphs with the ones obtained with the SF (fig. 6) in all the cases the errors are reduced and the scaling is excellent for all q values. In order to quantify the differences in the scaling, in fig. 8 we show the slopes which are our estimates of $H(q)$. We can now estimate $\zeta(q)$ and observed more clear than meanwhile June and July show a concave downwards shape (figs. 9a, 9b), December presents a closer linear pattern than using a SF method (fig. 9c).

TABLE II. – *Generalized Hurst exponents values (*$H(q)$*) from the two extremes,* $q = 0.5$ *and* $q = 6$*, and for* $q = 2$*.* ΔH *is the amplitude of variation of* $H(q)$*. Estimations have been made through the structure function (SF).*

	$H(0.5)$	$H(6)$	ΔH	$H(2)$
June	0.54 ± 0.08	0.17 ± 0.09	0.37	0.32 ± 0.06
July	0.58 ± 0.12	0.30 ± 0.05	0.27	0.42 ± 0.07
December	0.35 ± 0.05	0.22 ± 0.05	0.13	0.28 ± 0.03

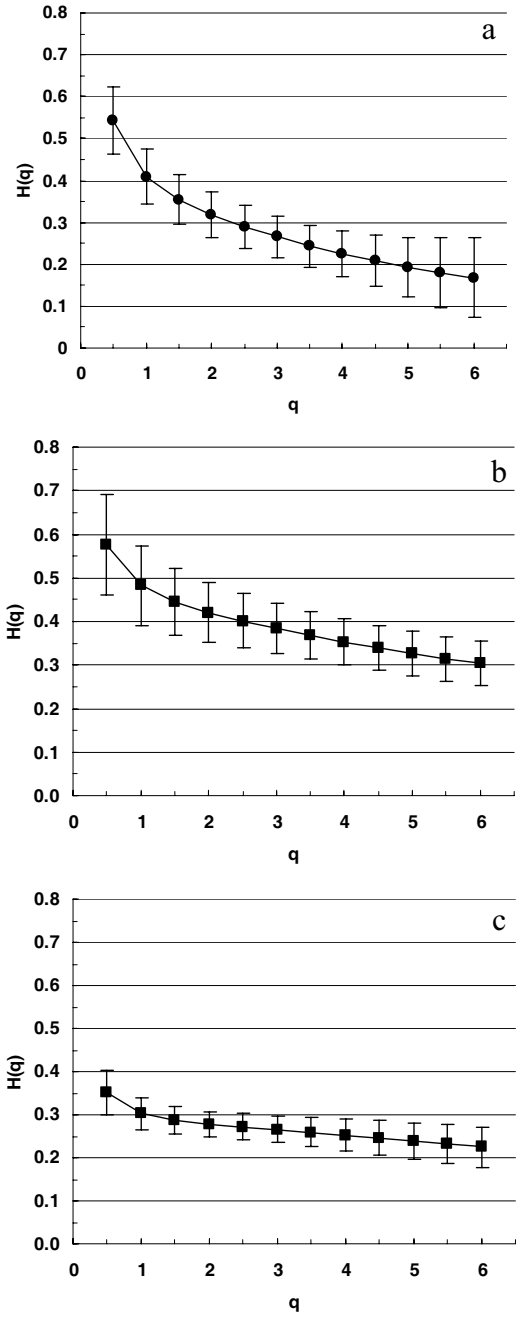

Fig. 6. – $H(q)$ curves obtained based on $\zeta(q)$ for a) June, b) July, c) December 2004.

Using the generalized exponent $H(q)$ we quantify again the range of variation of $H(q)$ values ($H(0.5)$–$H(6)$) and the Hurst exponent ($H(2)$) estimated. In table III Hurst exponent presents a clear anti-persistent character as shown earlier in table II. However,

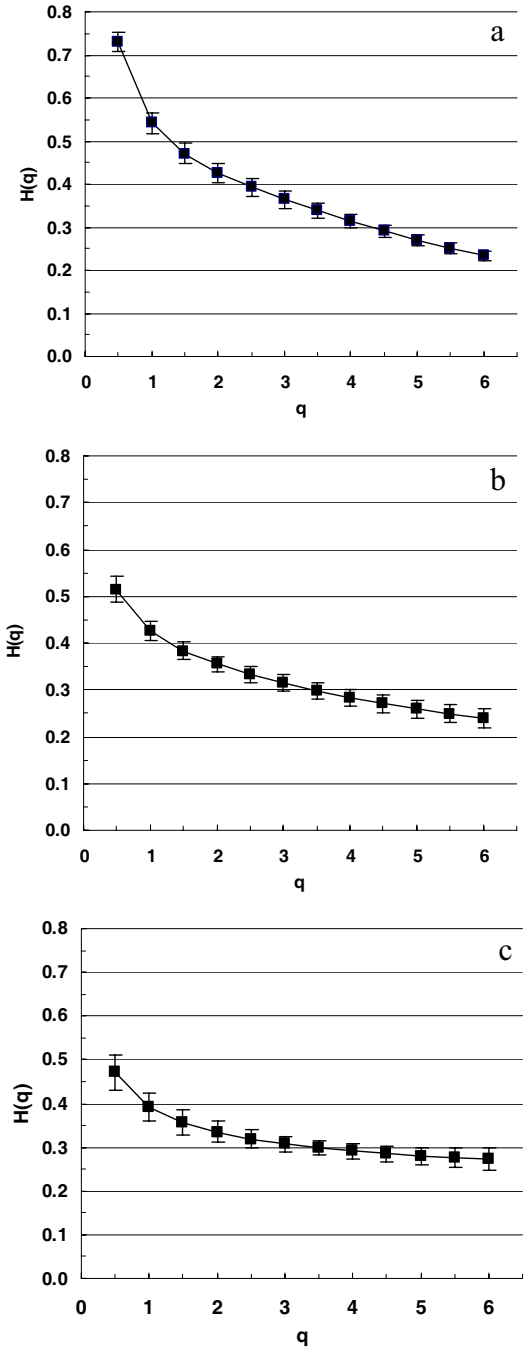

Fig. 7. – $H(q)$ curves obtained by Detrended Fluctuation Analysis (DFA) for a) June, b) July, c) December 2004.

the amplitudes of $H(q)$ and the $H(2)$ values have changed and present lower errors making the comparison more suitable. The month of June presents the higher amplitude and

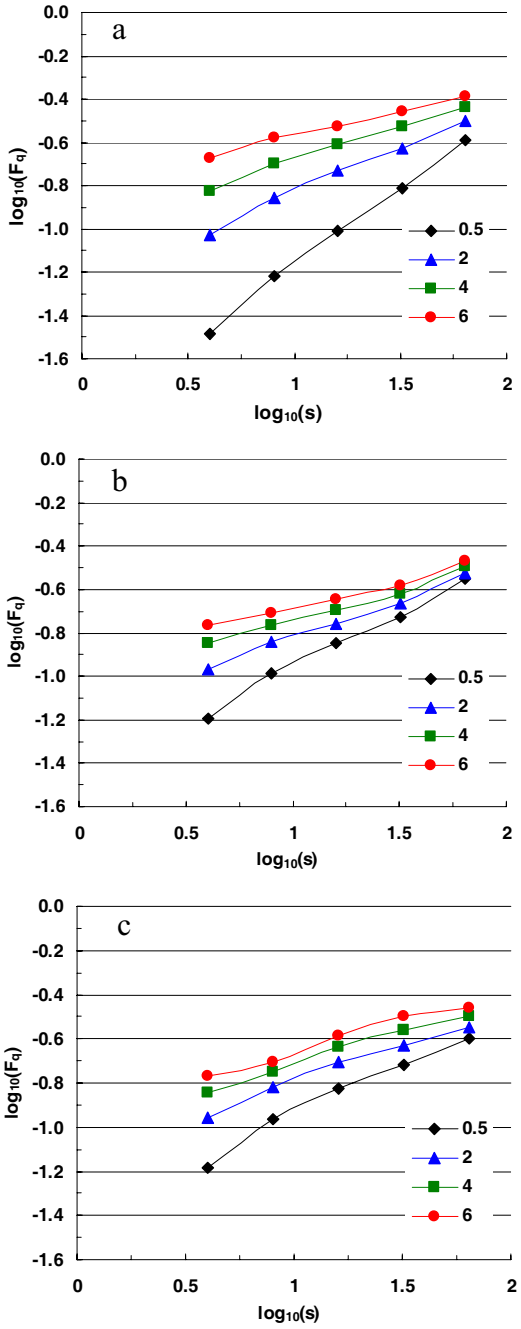

Fig. 8. – Detrended fluctuation (F_q) for $q = 0.5$, 2, 4 and 6 for (a) June, (b) July and (c) December 2004.

higher Hurst exponent, all of them being less than 0.5. Comparing the errors showed in table II with these ones the reduction using DFA is almost half pointing out the benefit of using this method.

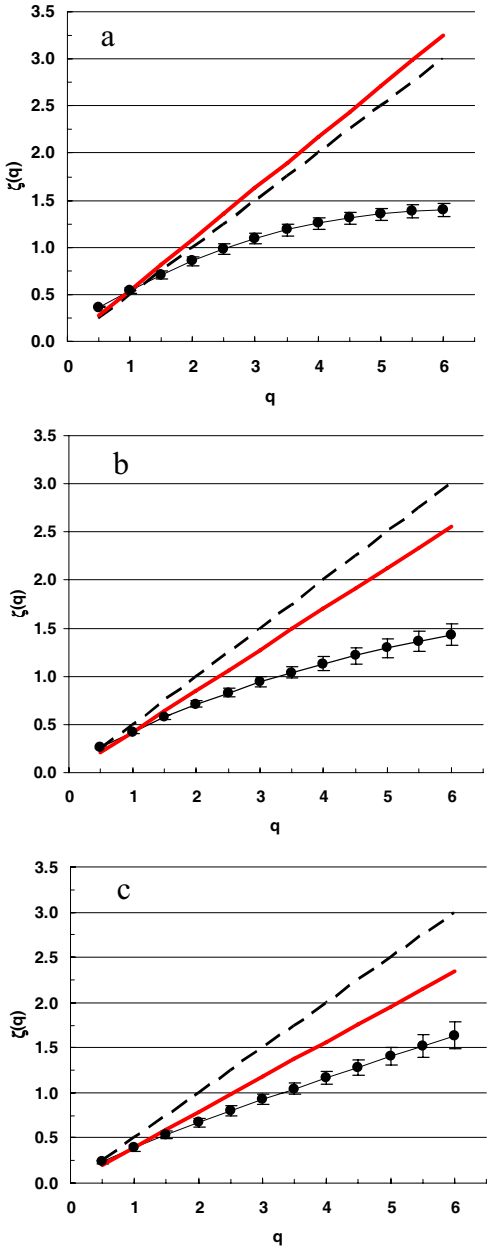

Fig. 9. – $\zeta(q)$ curves obtained based on $H(q)$ for a) June, b) July, c) December. Dashed line represents time series with uncorrelated noise (slope value of 0.5), grey line represents the linear part of $\zeta(q)$ having a constant slope value of $\zeta(q = 1)$.

Finally the parameters extracted from $\zeta(q)$ can be observed in table IV. All H values are again higher than 1/3, although the estimation error is only of ± 0.03. We would like to point out at that even DFA was not necessary, as we saw in the SF section all $H(2)$ values were lower than 1, the application of this method has remarkably reduced the errors associated to the linear regression estimation.

TABLE III. – *Generalized Hurst exponents values* ($H(q)$) *from the two extremes,* $q = 0.5$ *and* $q = 6$*, and for* $q = 2$*.* ΔH *is the amplitude of* $H(q)$ *variation. Estimations have been made through detrended fluctuation analysis (DFA).*

	$H(0.5)$	$H(6)$	ΔH	$H(2)$
June	0.73 ± 0.02	0.23 ± 0.01	0.50	0.43 ± 0.02
July	0.52 ± 0.03	0.24 ± 0.02	0.28	0.36 ± 0.02
December	0.47 ± 0.04	0.27 ± 0.03	0.20	0.34 ± 0.02

TABLE IV. – $\zeta(q)$ *values from* $q = 1$ *(H),* $q = 4$ *and* $q = 6$*. Estimations have been made through detrended fluctuation analysis (DFA). Parameters estimated for intermittency* (μ) *and deviation from linear structure function* (λ)*.*

	$\zeta(q=1)$	$\zeta(q=4)$	$\zeta(q=6)$	μ	λ
June	0.54 ± 0.02	1.26 ± 0.06	1.40 ± 0.07	0.74 ± 0.06	0.91 ± 0.16
July	0.43 ± 0.02	1.13 ± 0.07	1.43 ± 0.12	0.87 ± 0.07	0.57 ± 0.16
December	0.39 ± 0.03	1.16 ± 0.07	1.64 ± 0.15	0.84 ± 0.07	0.40 ± 0.20

At the same time the errors at $\zeta(q = 4)$ are quite reduced being half in June and July reducing the uncertainty to the parameters based on this value (μ and λ). This gives a full meaning to the intermittent parameter μ, ranging from 0.87 (July) till 0.74 (June). At the same time, λ parameter shows a descending trend from June till December (see table IV).

5. – Conclusions

In summary, we have applied a multifractal (MF) analysis to wind series, registered each 10 minutes, corresponding to three different months using two methodologies. First, the structure function (SF) was applied obtaining $\zeta(q)$ and from this the generalized Hurst exponents ($H(q)$). Later, a detrended fluctuation analysis (DFA) was used to estimate $H(q)$ and then infer $\zeta(q)$. This comparison suggests that both methods allow a reliable multifractal characterization of multifractal nonstationary time series showing a general agreement in the results. However, MF DFA presents stronger statistical results due in part to error reduction in their estimations.

In all the months studied in this work the linear parameter H estimated from $\zeta(q)$ has been always different from classical Kolmogorov turbulent result of 1/3 or 0.33, varying from 0.39 to 0.54 when it was calculated with DFA. When they were estimated applying SF, H was closer to 1/3 in December. We have shown that using MF DFA an intermittent parameter can be estimated with lower uncertainty than using MF SF.

* * *

This work has been supported by CM (Spain) under Project Number CCG07-UPM/AMB-1998.

REFERENCES

[1] LAUREN M. K., MENDABE M. and AUSTIN G. L., *Boundary-Layer Meteorol.*, **100** (2001) 263.

[2] Burton T., Sharpe D., Jenkins N. and Bossanyi E., *Wind Energy Handbook* (John Wiley & Sons) 2001.
[3] Van der Hoven I., *J. Meteorol.*, **14** (1957) 160.
[4] Egglestone E. D. and Clark R. N., *Wind Eng.*, **24** (2000) 49.
[5] Lovejoy S., Schertzer D. and Stanway J. D., *Phys. Rev. Lett.*, **86** (2001) 5200.
[6] Yagüe C., Viana S., Maqueda G. and Redondo J. M., *Nonlinear Processes Geophys.*, **13** (2006) 185.
[7] Vindel J. M., Yagüe C. and Redondo J. M., *Nonlinear Processes Geophys.*, **15** (2008) 1.
[8] Bras R. and Rodríguez-Iturbe I., *Random Functions and Hydrology* (Dover Publications, Inc., New York) 1993.
[9] Davis A., Marshak A., Wiscombe W. and Cahalan R., *J. Geophys. Res.*, **99** (1994) 8055.
[10] Tuck A. F. and Hovde S. J., *Geophys.-Res.-Lett.*, **26** (1999) 1271.
[11] Tarquis A. M., Castellanos M. T., Morató M. C. and Antón J. M., *WSEAS Trans. Syst.*, **5** (2006) 605.
[12] Kavasseri R. G. and Nagarajan R., *Chaos, Solitons Fractals*, **24** (2004) 165.
[13] Frisch U. and Parisi G., *A Multifractal Model of Intermittency in Turbulence and Predictability*, in *Geophysical Fluid Dynamics and Climate Dynamics* (North-Holland, Amsterdam) 1985, pp. 84-88.
[14] Frisch U., *Turbulence, The Legacy of A. Kolmogorov* (Cambridge University Press, Cambridge, UK) 1995.
[15] Meneveau C. and Sreenivasan K. R., *Phys. Lett. A*, **137** (1989) 103.
[16] Schmitt F., Schertzer D., Lovejoy S. and Brunet Y., *Fractals*, **1** (1993) 568.
[17] Lovejoy S. and Schertzer D., *J. Geophys. Res.*, **95** (1990) 2021.
[18] Marshak A., Davis A., Cahalan R. F. and Wiscombe W. J., *Phys. Rev. E*, **49** (1994) 55.
[19] Schertzer D. and Lovejoy S., *Geophys. Monogr. Ser.*, **150** (2005) 317.
[20] García J. L., de la Plaza S., Navas L., Benavente R. M. and Luna L., *J. Agric. Eng. Res.*, **69** (1998) 107.
[21] Bailey B. J. and Chalabi Z. S., *Comput. Electron. Agric.*, **10** (1994) 203.
[22] Bailey B. J., *Acta Hort. (ISHS)*, **534** (2000) 21.
[23] Schertzer D. and Lovejoy S., *J. Geophys. Res.*, **92** (1987) 9693.
[24] Kantelhardt J. W., Zscchegner S. A., Koscielny-Bunde K., Havlin S., Bunde A. and Stanley E., *Physica A*, **316** (2002) 87.
[25] Fernandez J. and Aguado P. L., *Datos Meteorológicos 1990-1992. Estación Meteorológica de Botánica Agrícola*, edited by E.T.S.I.A. Ciudad Universitaria de Madrid (U.P.M.) 1993.
[26] Jangamshetty S. H. and Rau V. G., *IEEE Trans. Energy Conver*, **14** (1999) 1537.
[27] Feder J., *Fractals* (Plenum Press, New York) 1988.
[28] Hurst H. E., *Proc. Am. Soc. Civil Eng.*, **116** (1951) 770.
[29] Yu C. X., Peebles W. A. and Rhodes T. L., *Plasma Turbulence*, **10** (2003) 2772.
[30] Gilmore M., Yu C. X., Rhodes T. L. and Peebles W. A., *Plasma Turbulence*, **9** (2002) 1312.
[31] Moody J. and Wu L., *Long memory and hurst exponents of tick-by-tick interbank foreign exchange rates*, *Proc. Comput. Intell. Financial Eng.* (IEEE Press, Piscataway, NJ) 1995, pp. 26-30.
[32] Weron R. and Przybylowicz B., *Physica A*, **283** (2000) 462.
[33] Erramilli A., Roughan M., Veitch D. and Willinger W., *Proc. IEEE*, **90** (2002) 800.
[34] Ivanov P. C., Amaral L, Goldberger A., Havlin S., Rosenblum M. G., Struzik Z. R. and Stanley H. E., *Nature*, **399** (1999) 461.
[35] Beran J., *Statistics for Long Memory Processes* (Chapman and Hall, New York) 1994.
[36] Bassingthwaighte J. B., Liebovitch L. S. and West B. J., *Am. Physiol. Soc., Oxford*, (1994) 78.

[37] Kolmogorov A. N., *Dokl. Akad. Nauk. SSSR*, **32** (1941) 19.
[38] Sreenivasan K. R. and Antonia R. A., *Annu. Rev. Fluid Mech.*, **29** (1997) 435.
[39] Mahjoub O. B., Babiano A. and Redondo J. M., *Flow, Turbulence and Combustion*, **59** (1998) 299.
[40] Mahrt L., *J. Atmos. Sci.*, **46** (1989) 79.
[41] Katul G. G., Parlange M. B. and Chu C. R., *Phys. Fluids*, **6** (1994) 2480.
[42] Holschneider M., *Wavelets an Analysis Tool* (Oxford Science Publications) 1995.
[43] Bacry E., Muzy J. F. and Arneodo A., *J. Stat. Phys.*, **70** (1993) 635.
[44] Frisch U., Sulem P. L. and Nelkin M., *J. Fluid Mech.*, **87** (1978) 719.